



HAL
open science

Atmospheric dynamics and West European summer hot temperatures since 1871

M Carmen Alvarez-Castro, Davide Faranda, Pascal Yiou

► **To cite this version:**

M Carmen Alvarez-Castro, Davide Faranda, Pascal Yiou. Atmospheric dynamics and West European summer hot temperatures since 1871. 2016. hal-01370975v2

HAL Id: hal-01370975

<https://hal.science/hal-01370975v2>

Preprint submitted on 13 Dec 2016 (v2), last revised 23 Nov 2017 (v3)

HAL is a multi-disciplinary open access archive for the deposit and dissemination of scientific research documents, whether they are published or not. The documents may come from teaching and research institutions in France or abroad, or from public or private research centers.

L'archive ouverte pluridisciplinaire **HAL**, est destinée au dépôt et à la diffusion de documents scientifiques de niveau recherche, publiés ou non, émanant des établissements d'enseignement et de recherche français ou étrangers, des laboratoires publics ou privés.

1 Atmospheric dynamics and West European summer 2 hot temperatures since 1871

3 M. Carmen Alvarez-Castro, Davide Faranda, Pascal Yiou

4 Laboratoire des Sciences du Climat et de l'Environnement, UMR 8212

5 CEA-CNRS-UVSQ, IPSL, Université Paris-Saclay, F-91191 Gif-sur-Yvette, France

6 E-mail: carmen.alvarez-castro@lsce.ipsl.fr

7 December 2016

8 **Abstract.** Summer hot temperatures have many impacts on health, economy
9 (agriculture, energy, transports) and ecosystems. In western Europe, the recent
10 summers of 2003 and 2015 were exceptionally warm. Many studies have shown that
11 the genesis of the major heat events of the last decades was linked to anticyclonic
12 atmospheric circulation and to spring precipitation deficit in southern Europe. Such
13 results were obtained for the second part of the 20th century and projections into the
14 21st century. In this paper, we challenge this vision by investigating the earlier part
15 of the 20th century from an ensemble of 20CR reanalyses. We propose an innovative
16 description of Western-European heat events that takes into account the dynamics of
17 the circulation. We argue that the atmospheric circulation patterns leading to the
18 most intense heat events have changed during the last century. We also show that the
19 increasing temperature trend during major heatwaves is encountered during episodes
20 of Scandinavian blocking, while other circulation patterns do not yield temperature

21 trends during extremes.

22 *Keywords:* Weather Regimes, Climate Dynamics, Heat Events

23 **1. Introduction:**

24 In western Europe, recent hot summers were characterized by highly anomalous
25 meteorological conditions. In these situations, such as 2003, the heat was prolonged
26 and intense, and the consequences were disastrous for society and ecosystems (Schär &
27 Jendritzky 2004, Robine et al. 2008, Wreford & Adger 2010, Poumadere et al. 2005, Ciais
28 et al. 2005).

29 European surface temperature variations are influenced by processes that combine
30 radiative forcing, the large-scale atmospheric circulation and local phenomena. Over
31 the last five decades, most of the intense European heat events have been connected
32 to prolonged spells of anticyclonic circulation (Scandinavian blocking) and dry spring
33 conditions in Southern Europe (Schär et al. 1999, Fischer et al. 2007, Mueller &
34 Seneviratne 2012, Zampieri et al. 2009, Quesada et al. 2012, Vautard et al. 2007).
35 However, the Summer 2011 was cool and preceded by a dry spring; the Summer 2013
36 was warm and preceded by a wet spring; and the Summer 2015 was warm with persisting
37 southerly atmospheric flows and no lasting blocking episodes. The goal of this paper is
38 to assess the robustness of the link between heat events and atmospheric circulation. We
39 perform a statistical and dynamical analysis on a long period that covers 1871–2015.
40 Since anticyclones extend to a radius of few hundreds kilometers, such a connection

41 must be investigated on a regional scale (Della-Marta et al. 2007, Stefanon et al. 2012).
42 Hence, we restrict our analysis to Western Europe in the region covering France and the
43 Iberian Peninsula, whose weather conditions are strongly influenced by the atmospheric
44 circulation over the North Atlantic. This analysis also puts some of the results of Horton
45 et al. (2015) on this link into a broader time perspective.

46 **2. Data and Methods:**

47 We base our analysis on the sea-level pressure (SLP) and the surface temperature fields
48 during summers (June-July-August: JJA) in 20th Century Reanalysis data (20CR:
49 1871–2011, (Compo et al. 2011)). To ensure the robustness of the results, we used
50 the ensemble mean (EM) and 10 members (M0-M9) of the ensemble. The analysis is
51 completed with other reanalysis products: NCEP (1948–2015) (Kalnay et al. 1996) and
52 ERA20C reanalysis (1900–2000) (Poli et al. 2013) (see supplementary material). In order
53 to describe the variability of the atmospheric circulation, we decompose the summer SLP
54 anomalies field (obtained by removing the seasonal cycle) into four weather regimes
55 following the approach of Yiou et al. (2008) and study their connection with heat events
56 at seasonal(i) and sub-seasonal(ii) timescales in Western-Europe [$10^{\circ}\text{W} - 7.5^{\circ}\text{E}$; $35 -$
57 50°N]. i) Seasonal: the 20 summers with high mean temperature anomalies of the period
58 1871–2011, and ii) Subseasonal: heatwaves defined as periods with high temperatures
59 anomalies for at least five consecutive days. In both analyses temperatures are detrended
60 by removing a linear trend calculated from the time series of summer seasonal means.

61 The goal of the detrending is to remove the effect of the well-documented European
62 temperature increase, which does not depend on the weather pattern.

63 *2.1. Weather Regimes:*

64 Weather regimes are recurring states of the atmospheric circulation and provide a useful
65 description of the atmospheric variability (Michelangeli et al. 1995, Corti et al. 1999).
66 Following the methods of Michelangeli et al. (1995) and Yiou et al. (2008) we compute
67 four weather regimes over the North Atlantic region [80°W – 50°E; 20 – 70°N] (Fig.
68 1a-d) using the first ten Empirical Orthogonal Functions (EOFs), which calculated on
69 daily NCEP SLP anomalies (reference period: 1970–2010) over the summers (JJA). To
70 weigh the variations of the grid cell surface, the data are normalized by the square root
71 of cosine of latitude. The k-means algorithm (Michelangeli et al. 1995) is applied to
72 the ten first EOFs of the SLP anomalies to compute the four cluster centroids. The
73 Principal Components centroids are recomposed with the EOFs to obtain the weather
74 regimes in physical space. For comparison, we classify different reanalysis datasets with
75 the NCEP weather regimes. All the reanalysis data are interpolated onto the NCEP grid
76 ($2.5^\circ \times 2.5^\circ$). The SLP data classifications of all reanalyses are obtained by determining
77 the minimum of the Euclidean distances to the four NCEP summer weather regime cen-
78 troids. This is achieved without further EOF truncation. The NCEP summer weather
79 regimes are shown in Fig. 1a-d, with the same nomenclature as in Cassou et al. (2005):
80 a) the negative phase of North Atlantic Oscillation (NAO–) showing a dipole between

81 Greenland and Northern Europe, b) the Atlantic Ridge (AR), with a high pressure over
82 the center of the North Atlantic and some common features with the positive phase of
83 NAO, c) Scandinavian Blocking (BLO), with a high pressure center over Scandinavia,
84 d) Atlantic Low (AL), with a low pressure center covering the central North Atlantic.

85

86 To ensure that there are no inhomogeneities in the method, we have verified that
87 the RMSE between the reference period and the other periods/datasets is small (Fig.
88 S8).

89 *2.2. Projection onto weather regimes for a dynamical representation:*

90 In order to visualize the dependence between the daily SLP fields and the four weather
91 regimes, we represent the *trajectory* of each summer in the space of correlations (Fig.
92 2a-c) using an approach based on dynamical systems theory (Katok & Hasselblatt 1997)
93 . In this framework, the motion of a particle is represented in the space defined by its
94 position and speed (the so-called phase space). In our set-up, the particle is replaced
95 by a SLP field and the directions in phase space correspond to the projections on the
96 four weather regimes. Trajectories provide additional information with respect to the
97 monthly average statistical quantities, on the time dependence and the coherence of
98 the dynamical projection with respect to weather regime bases. If a trajectory jumps
99 every day to a different region of the phase space, then a dominant weather regime is
100 not representative of the dynamical behavior of events lasting several days. If instead

101 the trajectory occupies a restricted region of the phase space with smooth transitions of
102 the projection among weather regimes, then the dynamical representation is informative
103 and the base of weather regimes is appropriate.

104 This is equivalent to assuming the existence of a low-dimensional attractor. The
105 caveat is that the weather regime description is a first order simplification of the
106 atmospheric circulation that captures large scale features. Although this phase-
107 space method has been debated since Lorenz (1991), there are theoretical (Chekroun
108 et al. 2011) and experimental (Casdagli et al. 1991) evidences that such a procedure is
109 effective when the dynamics can be projected on a low dimensional phase space with a
110 stochastic perturbation.

111 **3. Results and Discussion:**

112 The link between the North Atlantic atmospheric circulation and heat events over France
113 and the Iberian Peninsula is investigated at two timescales.

114 *3.1. Seasonal scale: weather regimes during the warmest summers*

115 We carried out a statistical analysis of the 20 hottest summers of the period 1871–2011
116 (Fig. 1i). In Western-Europe [$10^{\circ}\text{W} - 7.5^{\circ}\text{E}$; $35 - 50^{\circ}\text{N}$], the 20 hottest summers (Fig.
117 1i and 2) are defined in each dataset as the ones having the highest average temperature
118 anomalies with respect to the climatology. Figure 1e-h shows the anomalous summer
119 frequency of weather regimes in 20CR with respect to the NCEP reference period. In

120 this figure we see how NAO- is the unique regime decreasing in frequency with the
121 time, and BLO is the one increasing in frequency with the time. Figure 1i shows the
122 dominant regime as the one with the highest anomalous frequency. We find a general
123 agreement between all the 20CR members and the EM in terms of warmest summers
124 and the dominating weather regime. Most of the warmest summers (largest circles in
125 Fig. 1i) occur during the second part of the 20th century. As observed by Stott et al.
126 (2004) and Meehl & Tebaldi (2004), they also increase in frequency over time. Our
127 analysis shows significant changes in the dominating weather regimes associated with
128 warmest summers. If BLO is dominant from the second part of 20th century, scarce
129 occurrences of this weather regime are found before 1930, even within the ensemble
130 members of 20CR. BLO and AL regimes are conducive to warm extremes and NAO-
131 and AR are the opposite (Cassou et al. 2005). Figure 1i shows that, after 1930, it is
132 more frequent to find hottest summers linked to what we know as warm regimes. BLO
133 (the most frequent one after 1930) leads to stagnant air and potential land-surface feed-
134 backs, whereas AL relies on advection from lower latitudes. In the other hand, NAO-
135 is the dominant weather regime during warmerst summers up to 1930. This weather
136 regime contributes to a weakening of the westerly flow from the Atlantic into Western
137 Europe. AR regime is more stable in time (Figure 1f, 1i).

138

139 To understand such trends we decompose the average information found with the
140 statistical analysis via the dynamical representation of the warmest summers, defined in

141 section 2.2. We project the SLP anomaly fields onto NAO– and AR regimes, which are
142 the most frequent for the first part of the 20th century as shown in Fig. 1 e. This analysis
143 synthesizes the trajectory of the atmospheric circulation during heat events in a space
144 represented by the weather regimes. Consistently with the previous analysis, we find
145 that the atmospheric dynamics has evolved from patterns that are positively correlated
146 with NAO– during the late 19th century (Fig. 2 a), to negative correlations during the
147 rest of the record (Fig. 2 b-c). Similar projections on BLO and AL regimes show: that
148 BLO has the opposite change of NAO-, being negative during the first period (Figure
149 S4a) and positive during the last one (Figure S4c). AR and AL regimes do not show
150 significant differences between the periods. Those correlations add a daily temporal
151 information that is not captured by the analysis of the dominating seasonal weather
152 regime (Figure 1i) and highlight a change of atmospheric behavior. Thus the dominant
153 weather regime is a valid concept as the trajectories of heatwaves persist at sub-seasonal
154 scales around the same region of the phase space. These changes are consistent within
155 the 20CR ensemble, as the M0-M9 average (Fig. 2d) shows consistent results with the
156 EM.

157 *3.2. Subseasonal scale: weather regimes during heatwaves events*

158 To understand whether those results hold also for short time events (at least 5
159 consecutive days), independently from the fact that they have been observed during
160 hot summers, we compute the average temperature during heatwaves striking Western-

161 Europe.

162 Heatwave events are defined when the summer temperature exceeds a threshold
163 /percentiles (P90, P95) for more than 5 consecutive days. Figure 3 shows heatwave
164 events above the P90 threshold, computed on the area temperature anomalies (France
165 and the Iberian Peninsula). Temperatures in figure 3 are average values during each
166 heatwave event. Heatwaves events are grouped by the dominating weather regime. We
167 find that 19% of total events are dominated by NAO– (Fig. 3a), 36%, by BLO (Fig.
168 3c). Heatwaves that are associated by AR (Fig. 3b) and AL (Fig. 3d) weather regimes
169 have a frequency of 19% and 26%, respectively. Summer heatwave events dominated
170 by BLO regime have an increasing trend of $0.12^{\circ}\text{C}/\text{decade}$ along the period reaching
171 temperatures up to 29°C in the beginning of the 21st century. We also find that the
172 longest events are associated to BLO regime (Fig. 3e). On the contrary, NAO– have a
173 decreasing trend of $-0.06^{\circ}\text{C}/\text{decade}$ reaching 26°C at the end of the 19th century, and
174 24°C in the beginning of the 21st century. BLO is the only one with a significant trend
175 (p-values in Table S2, supplementary material).

176 To shed more light on the circulaion changes, we compute composites of SLP
177 and surface temperature anomalies for pre-1930 heatwaves (figure 4a) and post-1930
178 heatwaves (4c) during all the heatwave events found in analysis of figure 3. The exercise
179 is repeated by taking into account the occurrence of NAO– heatwave events for pre-1930
180 (4b) and the occurrence of BLO heatwave events for post-1930 (4d). The temperature
181 pattern changes in pre and post 1930 maps mainly in Greenland and the East coast

182 of North America and in Europe. Pressure patterns for all the heatwave events pre
183 and post-1930 reproduce well NAO– and BLO (respectively) albeit weaker for the BLO
184 regime. So, even if there is a change for NAO–, BLO is the one with a stronger change
185 for short-term events, because it is the most representative pattern in heatwaves events
186 from 1930.

187 **4. Conclusions:**

188 These results confirm that most heat events (either warmest summers and heatwaves in
189 Western Europe) of the second half of the 20th century occurred when the Scandinavian
190 Blocking weather regime dominated the North Atlantic region, causing increasing
191 temperatures and more frequent and longer heatwaves events (figure 3 and figure S7).
192 Our results also show that NAO– is more favorable to drive warm summers before 1930.
193 This early period corresponds to the most frequent co-occurrence of this regime and
194 heatwaves events. Although the increasing temperature trends observed during blocking
195 heatwaves episodes could be attributed to secular climate change (Coumou et al. 2014),
196 the change in the dominating weather regimes may have a different explanation, e.g.
197 the decadal variability of the atmospheric dynamics. Those findings are consistent with
198 the results of Horton et al. (2015), although we consider heatwaves on a finer spatial
199 scale (Western-Europe).

200 The robustness of our results is ensured by the use of 20CR ensemble and other
201 reanalysis datasets (see supplementary material). The dynamical analysis also suggests

202 that there is an increase of negative correlations between warmest summers and the
203 NAO– regime.

204 Although the information extracted in warmest summers and heatwaves is a priori
205 different, our analysis shows similar results at different timescales. In terms of warmest
206 summers, NAO– was the most representative pattern up to 1930 and from 1930 on, and
207 BLO is the most representative one. For short time heat events, the most representative
208 is BLO during the whole period but, as for warmest summers, NAO- events are less
209 frequent after 1930. BLO is associated to the longest and hottest heatwaves and yields
210 an increasing trend, as outlined by Horton et al. (2015).

211 In the debate on the mechanisms leading to changes in the atmospheric circulation
212 (Shepherd 2014), our results demonstrate the signature of the impacts of the atmospheric
213 circulation on European heat events.

214 **Acknowledgments:**

215 M.C.A-C. was supported by the Swedish Research Council grant No. C0629701
216 (MILEX). D.F. was supported by the ERC grant No. 338965–A2C2. P.Y. was sup-
217 ported by the European Unions Seventh Framework Programme grant No. 607085–
218 EUCLEIA. The authors thank G. Compo, for the help supported with data from
219 members of 20CR reanalysis. 20CR and NCEP Reanalysis data provided by
220 the NOAA/OAR/ESRL PSD, Boulder, Colorado, USA, from their Web site at
221 <http://www.esrl.noaa.gov/psd/>. ERA-20C reanalysis data provided by the ECMWF

222 (European Centre for Medium-Range Weather Forecasts), Reading, UK, from their
223 website at <http://apps.ecmwf.int/datasets/data/era20c-daily/>.

224

225 **Supplementary information:**

226 Available in the online version of the paper. Correspondence and requests for materials
227 should be addressed to M.C.A-C (email: carmen.alvarez-castro@lsce.ipsl.fr).

228 **References:**

- 229 Casdagli, M., Eubank, S., Farmer, J. D. & Gibson, J. (1991). State space reconstruction in the presence
230 of noise, *Physica D.* **51**(1): 52–98.
- 231 Cassou, C., Terray, L. & Phillips, A. S. (2005). Tropical atlantic influence on European heat waves, *J.*
232 *Climate* **18**(15): 2805–2811.
- 233 Chekroun, M. D., Simonnet, E. & Ghil, M. (2011). Stochastic climate dynamics: Random attractors
234 and time-dependent invariant measures, *Physica D.* **240**(21): 1685–1700.
- 235 Ciais, P. et al. (2005). Europe-wide reduction in primary productivity caused by the heat and drought
236 in 2003, *Nature* **437**(7058): 529–533.
- 237 Compo, G. P. et al. (2011). The twentieth century reanalysis project, *Q. J. Roy. Meteor. Soc.*
238 **137**(654): 1–28.
- 239 Corti, S., Molteni, F. & Palmer, T. (1999). Signature of recent climate change in frequencies of natural
240 atmospheric circulation regimes, *Nature* **398**(6730): 799–802.
- 241 Coumou, D., Petoukhov, V., Rahmstorf, S., Petri, S. & Schellnhuber, H. J. (2014). Quasi-resonant
242 circulation regimes and hemispheric synchronization of extreme weather in boreal summer,
243 *Proceedings of the National Academy of Sciences* **111**(34): 12331–12336.

- 244 Della-Marta, P. M., Luterbacher, J., von Weissenfluh, H., Xoplaki, E., Brunet, M. & Wanner, H. (2007).
245 Summer heat waves over western Europe 1880–2003, their relationship to large-scale forcings
246 and predictability, *Clim. Dynam.* **29**(2-3): 251–275.
- 247 Fischer, E., Seneviratne, S., Lüthi, D. & Schär, C. (2007). Contribution of land-atmosphere coupling
248 to recent European summer heat waves, *Geophys. Res. Lett.* **34**(6).
- 249 Horton, D. E., Johnson, N. C., Singh, D., Swain, D. L., Rajaratnam, B. & Diffenbaugh, N. S. (2015).
250 Contribution of changes in atmospheric circulation patterns to extreme temperature trends,
251 *Nature* **522**(7557): 465–469.
- 252 Kalnay, E. et al. (1996). The NCEP/NCAR 40-year reanalysis project, *B. AM. Meteorol. Soc.*
253 **77**(3): 437–471.
- 254 Katok, A. & Hasselblatt, B. (1997). *Introduction to the modern theory of dynamical systems*, Vol. 54,
255 Cambridge University Press.
- 256 Lorenz, E. N. (1991). Dimension of weather and climate attractors, *Nature* **353**(6341): 241–244.
- 257 Meehl, G. A. & Tebaldi, C. (2004). More intense, more frequent, and longer lasting heat waves in the
258 21st century, *Science* **305**(5686): 994–997.
- 259 Michelangeli, P.-A., Vautard, R. & Legras, B. (1995). Weather regimes: Recurrence and quasi
260 stationarity, *J. Atmos. Sci.* **52**(8): 1237–1256.
- 261 Mueller, B. & Seneviratne, S. I. (2012). Hot days induced by precipitation deficits at the global scale,
262 *Proc. Natl. Acad. Sci.* **109**(31): 12398–12403.
- 263 Poli, P. et al. (2013). The data assimilation system and initial performance evaluation of the ecmwf
264 pilot reanalysis of the 20th-century assimilating surface observations only (ERA-20C), *ECMWF*
265 *ERA Rep* **14**: 59.
- 266 Poumadere, M., Mays, C., Le Mer, S. & Blong, R. (2005). The 2003 heat wave in France: dangerous
267 climate change here and now, *Risk Anal.* **25**(6): 1483–1494.
- 268 Quesada, B., Vautard, R., Yiou, P., Hirschi, M. & Seneviratne, S. I. (2012). Asymmetric European
269 summer heat predictability from wet and dry southern winters and springs, *Nature Clim. Change*

270 **2**(10): 736–741.

271 Robine, J.-M., Cheung, S. L. K., Le Roy, S., Van Oyen, H., Griffiths, C., Michel, J.-P. & Herrmann,

272 F. R. (2008). Death toll exceeded 70,000 in Europe during the summer of 2003, *C. R. Biol.*

273 **331**(2): 171–178.

274 Schär, C. & Jendritzky, G. (2004). Climate change: hot news from summer 2003, *Nature*

275 **432**(7017): 559–560.

276 Schär, C., Lüthi, D., Beyerle, U. & Heise, E. (1999). The soil-precipitation feedback: A process study

277 with a regional climate model, *J. Climate* **12**(3): 722–741.

278 Shepherd, T. G. (2014). Atmospheric circulation as a source of uncertainty in climate change

279 projections, *Nat. Geosci.* **7**(703-708).

280 Stefanon, M., D’Andrea, F. & Drobinski, P. (2012). Heatwave classification over Europe and the

281 Mediterranean region, *Environ. Res. Lett.* **7**(1): 014023.

282 Stott, P. A., Stone, D. A. & Allen, M. R. (2004). Human contribution to the European heatwave of

283 2003, *Nature* **432**(7017): 610–614.

284 Vautard, R., Yiou, P., D’andrea, F., De Noblet, N., Viovy, N., Cassou, C., Polcher, J., Ciais, P.,

285 Kageyama, M. & Fan, Y. (2007). Summertime European heat and drought waves induced by

286 wintertime Mediterranean rainfall deficit, *Geophys. Res. Lett.* **34**(7).

287 Wreford, A. & Adger, W. N. (2010). Adaptation in agriculture: historic effects of heat waves and

288 droughts on UK agriculture, *Int. J. Agric. Sustain.* **8**(4): 278–289.

289 Yiou, P. et al. (2008). Weather regime dependence of extreme value statistics for summer temperature

290 and precipitation, *Nonlinear Proc. Geoph.* **15**(3): 365–378.

291 Zampieri, M., D’Andrea, F., Vautard, R., Ciais, P., de Noblet-Ducoudré, N. & Yiou, P. (2009). Hot

292 European summers and the role of soil moisture in the propagation of mediterranean drought,

293 *J. Climate* **22**(18): 4747–4758.

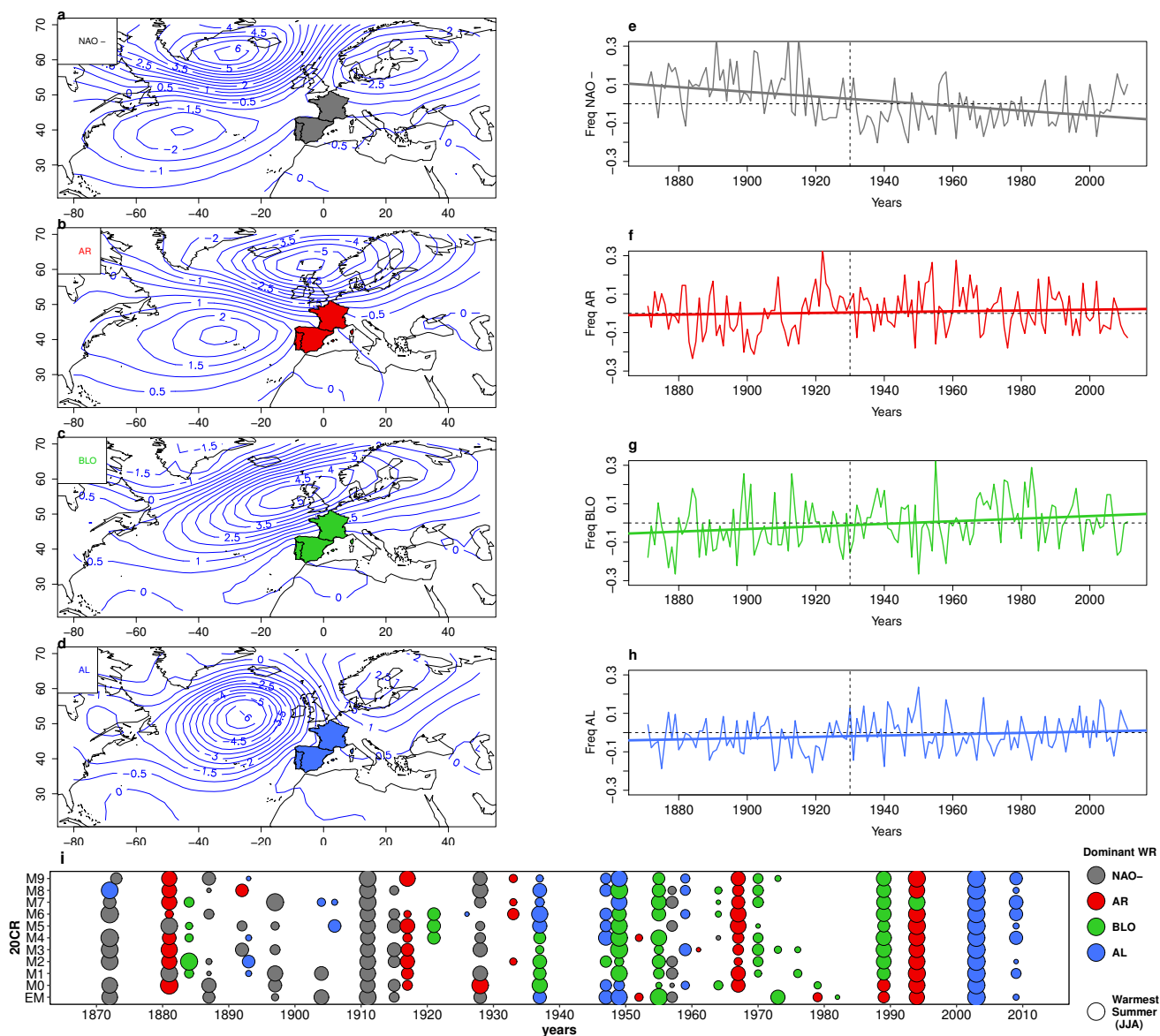


Figure 1. Summer SLP weather regimes over the North-Atlantic region and their dominance in the twenty warmest summers during 1871-2011 in Western-Europe. a-d, Summer SLP (hPa anomalies) Weather regimes: a, North Atlantic Oscillation in its negative phase (NAO-). b, Atlantic Ridge (AR). c, Blocking (BLO). d, Atlantic Low (AL) weather regime. e-h, Long-term weather regime frequency (anomalies) with respect the reference period (NCEP 1970-2010) i, Twenty warmest summers in Western-Europe (colored region in a-d) with their dominant weather regime. Years are shown in x axis, while y axis displays each of the 20CR members (M0 – M9) and the 20CR EM. Circle size depends on temperature (anomalies), the largest the warmest. Colors represents the dominant weather regime for each summer based in the highest anomalous frequency in e-h.

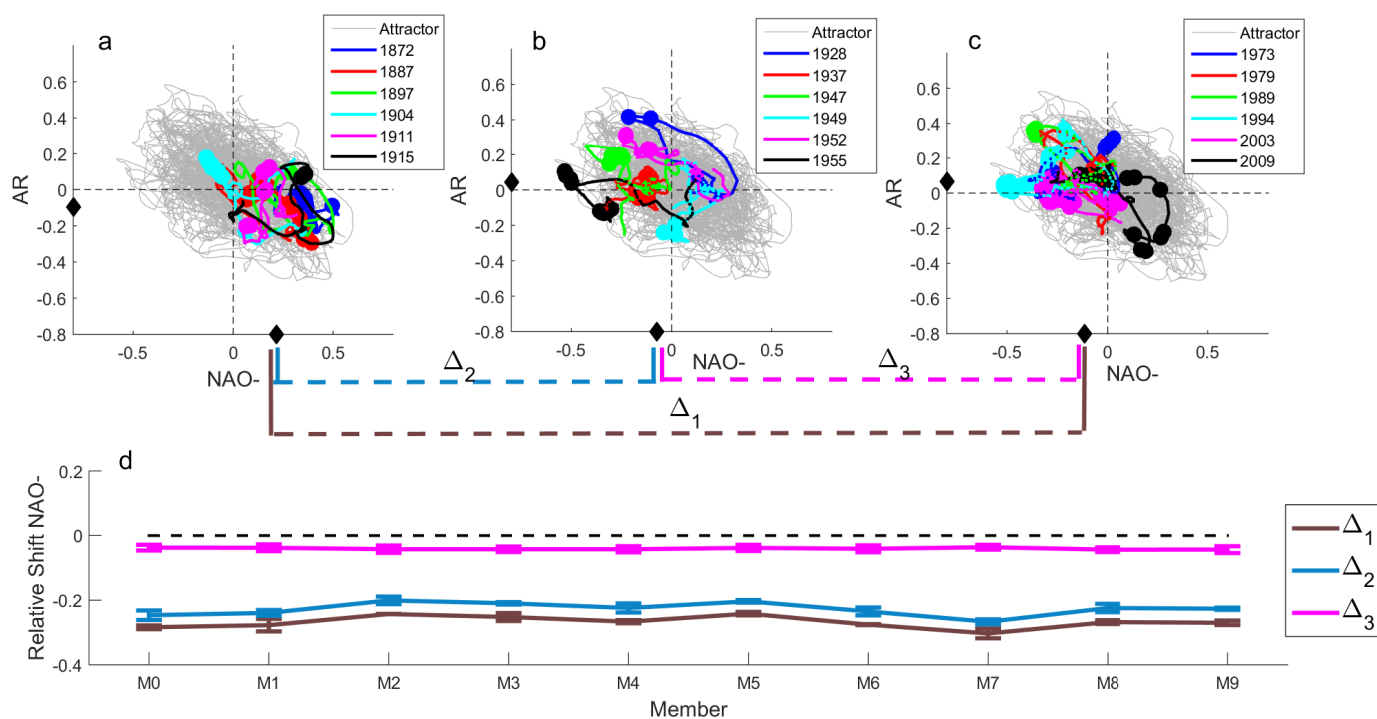


Figure 2. Dynamical representation of the warmest summers. a-c, Correlations of daily SLP fields and NAO- (x -axis), AR (y -axis) weather regimes for three different periods. Warmest summers are colored as in the legend, light grey lines represent all data. Big circles represent days with temperature above 85th percentile. Average correlations of warmest summers with respect to the NAO- weather regimes (black circle on x -axis) and relative difference between the periods ($\Delta_1 - 2 - 3$) for each member of the ensemble (d). Errorbars correspond to the standard deviation of the mean. A moving average filter with a 30 day window has been applied to the data.

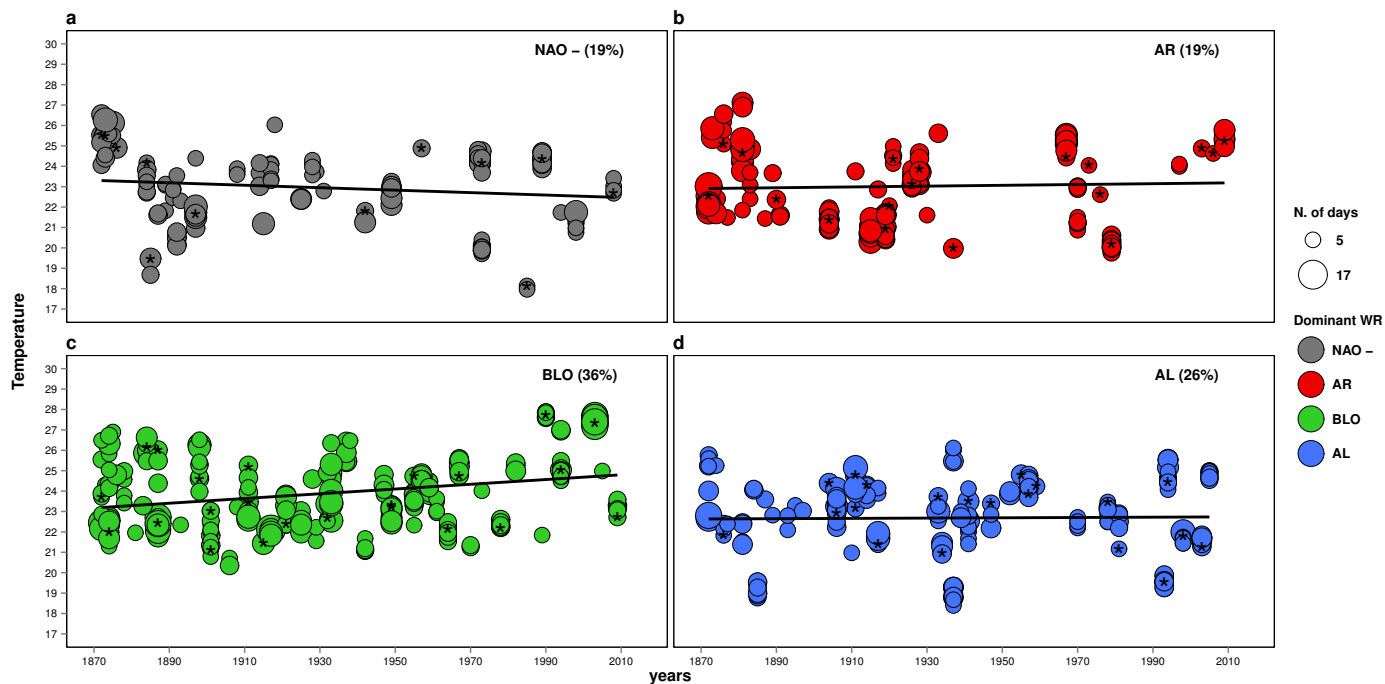


Figure 3. Dominant weather regimes during Summer heatwave events. In a–d, Summer heatwave events (90th Percentile) for members and EM (circles with stars) of 20CR data, 1871–2011. Colors correspond to the dominant weather regime in each event, temperature (y -axis) and years (x -axis). Circle sizes depend on the event duration by number of days, the larger the longer duration. Percentages show the frequency of each weather regime. Linear fits are shown in black solid lines.

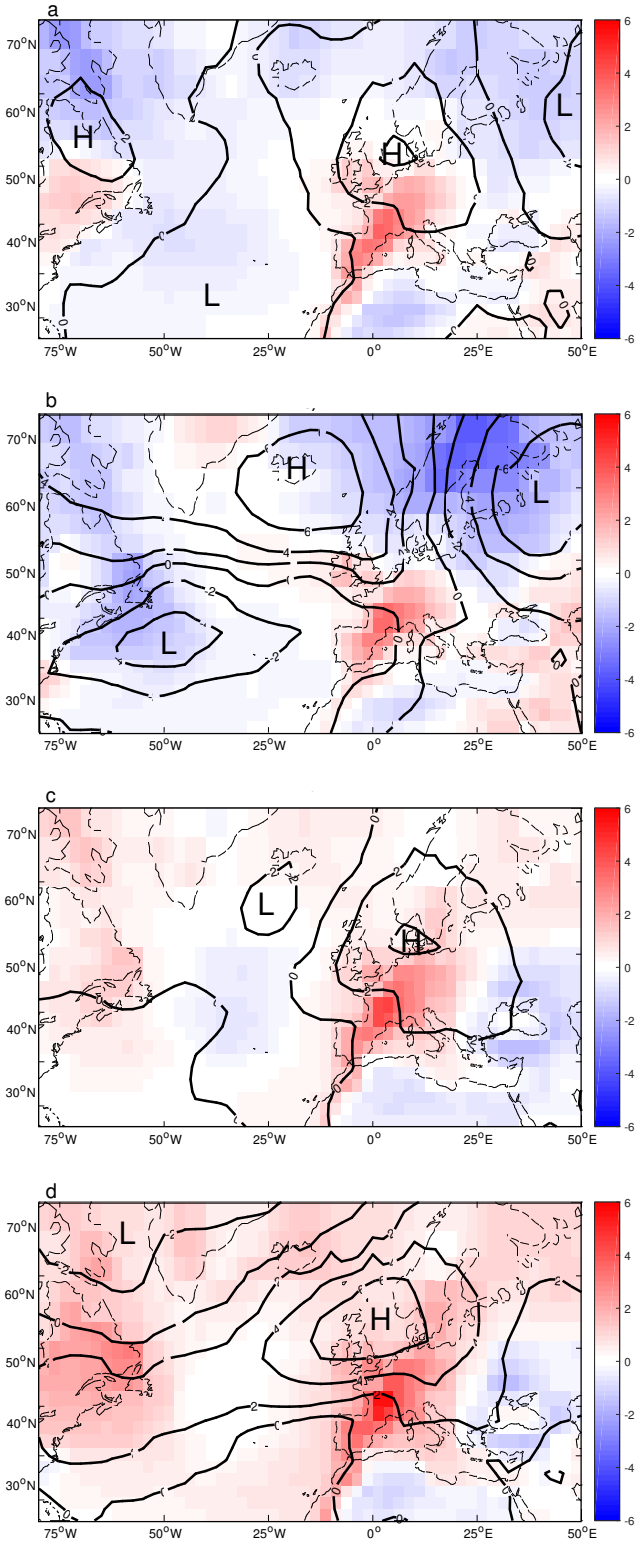


Figure 4. Composites of Sea Level Pressure (SLP) and Surface Temperature anomalies (SAT) pre/post 1930. In a–b, composites SLP (hPa) and SAT (°C) anomalies for a) all the days during heatwaves events found before 1930, in b) just the events where NAO- was the dominant weather regime. In c–d, composites SLP and SAT for c) all days during heatwaves events found after 1930, in d) just the events where BLO was the dominant regime.

1 Atmospheric dynamics leading to West European 2 summer hot temperatures since 1871

3 M. Carmen Alvarez-Castro, Davide Faranda, Pascal Yiou

4 Laboratoire des Sciences du Climat et de l' Environnement, UMR 8212

5 CEA-CNRS-UVSQ, IPSL, Université Paris-Saclay, F-91191 Gif-sur-Yvette, France

6 E-mail: carmen.alvarez-castro@lsce.ipsl.fr

7 December 2016

8 Supplementary Material

- 9 • Figure S1: Relative long-term summer weather regime frequency over the North-
10 Atlantic region and their dominance in warmest summers in Western-Europe (1871-
11 2015) using three reanalysis products (20CR, ERA20C, NCEP).
- 12 • Figure S2: Summer average temperatures for Western-Europe for three reanalysis
13 products (20CR, ERA20C, NCEP).
- 14 • Figure S3: Temperature anomalies during warmest summers (IP-France) with
15 dominance of each weather regime in three reanalysis products (20CR, ERA20C,
16 NCEP).
- 17 • Figure S4: Dynamical representation of the warmest summers for 20CR Ensemble

18 mean during 1871-2011 in regimes BLO-AL.

19 • Figure S5: Dynamical representation of the warmest summers for ERA20C during
20 1900-2010 in regimes AR-NAO- and BLO-AL.

21 • Figure S6: Dominant weather regimes during Summer Heatwave events in
22 Western-Europe for three reanalysis products (20CR, ERA20C, NCEP).

23 • Figure S7: Temperature (y-axis) vs numbers of days (x-axis) during each heatwave
24 event for the 20CR Ensemble Mean (1871-2011) weather regimes.

25 • Table S1: Absolute root mean square error by period and weather regime.

26 • Table S2: p-values of Heatwaves events in each dataset.

27 • Table S3: Average correlations for Fig2 with/without 30-days filter for each regime.

28 **References**

29 • Chambers, J. M. (1992). Linear models. Chapter 4 of *Statistical Models in S* eds
30 J. M. Chambers and T. J. Hastie, Wadsworth Brooks/Cole.

31 • Wilkinson, G. N. and Rogers, C. E. (1973). Symbolic descriptions of factorial
32 models for analysis of variance. *Applied Statistics*, **22**: 3929.

Atmospheric dynamics leading to West European summer hot temperatures since 18713

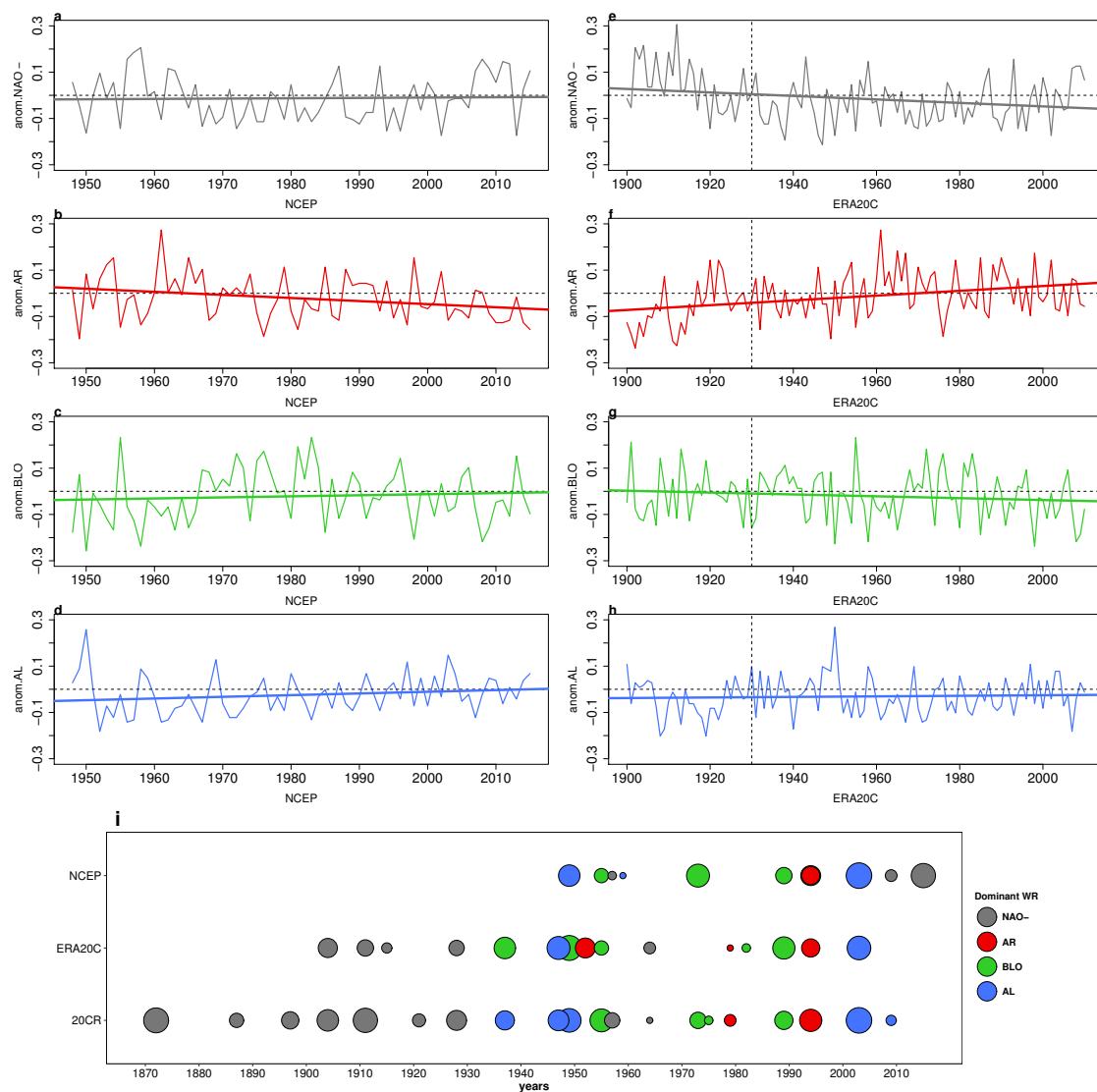


Figure 1. Relative long-term summer weather regime frequency over the North-Atlantic region and their dominance in warmest summers in Western-Europe (1871-2015) using three reanalysis products (20CR, ERA20C, NCEP). As in figure 1, relative frequency of Summer SLP (hPa anomalies) weather regimes: NAO- (a,e), AR (b,f), BLO (c,g) and AL (d,h), but considering NCEP data (a-d,) and ERA20C (e-h). e, Warmest summers from 1871 to 2015 in Western-Europe with their dominant weather regime. Years are shown in x axis while y axis display each of the reanalysis products (20CR, ERA20C, NCEP). Circle size depends on temperature anomalies, the largest the warmest. Colors (black, red, green, blue) represents the dominant weather regime (NAO-, AR, BLO, AL) for each summer. The number of warmest summers are ponderate with the length of each dataset.

Atmospheric dynamics leading to West European summer hot temperatures since 18714

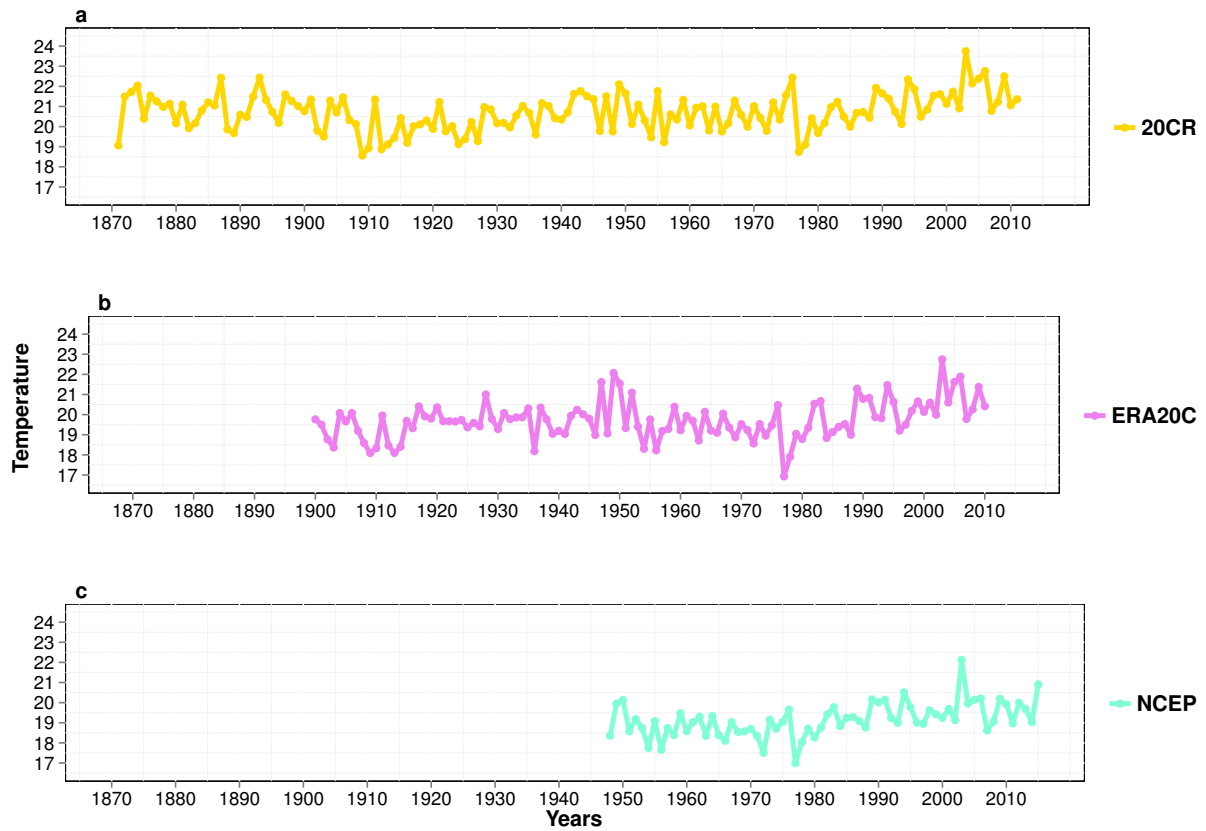


Figure 2. Summer average temperatures ($^{\circ}\text{C}$) for Western-Europe. a, 20CR b, ERA20C and c, NCEP).

Atmospheric dynamics leading to West European summer hot temperatures since 18715

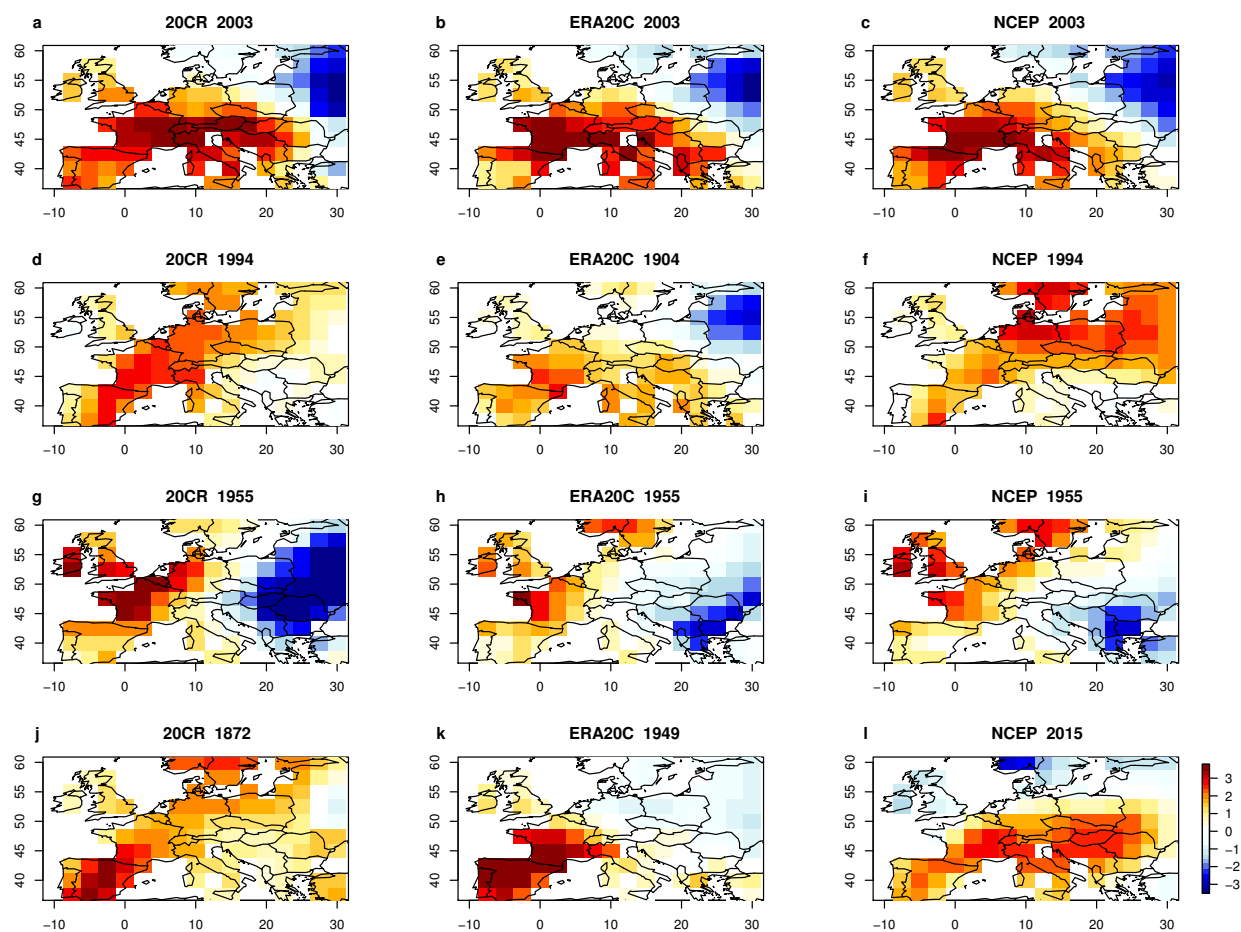


Figure 3. Temperature anomalies maps for warmest summers in Western-Europe. Each row correspond to a different dominant weather regime for some explanatory summers. Each column is a different reanalysis product. **a-c**, Summer 2003, where AL was the dominant weather regime. **d-f**, Summer of 1994, where AR was the dominant weather regime (Same frequencies of BLO and AR for NCEP during this summer). **g-i**, Summer of 1955, where BLO was the dominant weather regime. **j-l**, Since there is not a common summer for all the reanalysis datasets with NAO- as a dominant weather regime, here we show the most warmest summer (1872, 1904, 2015) where NAO- was the dominant weather regime in each reanalysis dataset (20CR, ERA20C, NCEP).

Atmospheric dynamics leading to West European summer hot temperatures since 18716

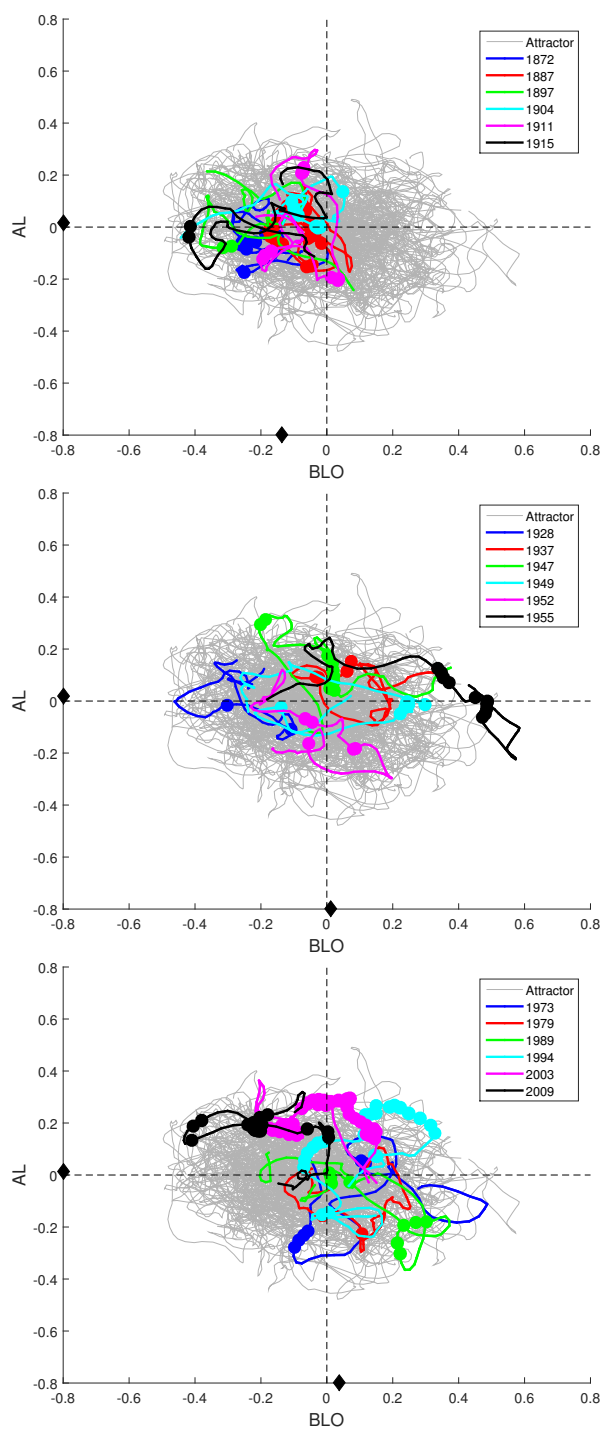


Figure 4. Dynamical representation of the warmest summers (same method as fig.2a-c in main text) for 20CR during 1871-2011. Correlations of daily SLP fields and BLO (x-axis), AL (y-axis) weather regimes for three different periods. Warmest summers are colored as in the legend, light grey lines represent all data. Big circles represent days with temperature above the 85th percentile. Average correlations of warmest summers with respect to each weather regime (black circle on x-axis).

Atmospheric dynamics leading to West European summer hot temperatures since 18717

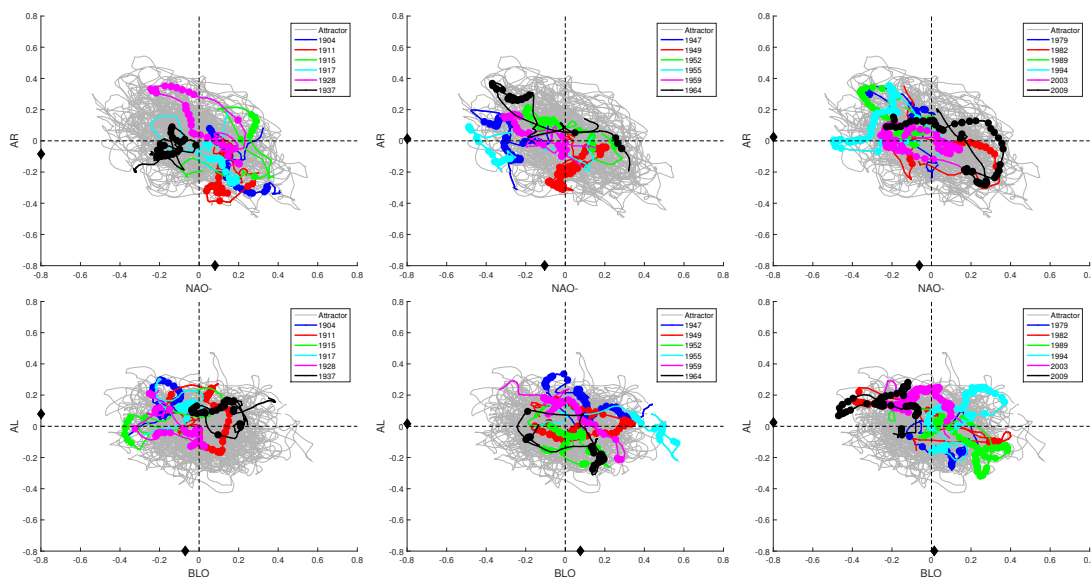


Figure 5. Dynamical representation of the warmest summers (same as fig.2a-c in main text) for ERA20C during 1900-2010. Correlations of daily SLP fields and NAO- (x-axis), AR (y-axis) weather regimes in upper panels and correlations of daily SLP fields and BLO (x-axis), AL (y-axis) weather regimes in the bottom panels for three different periods. Warmest summers are colored as in the legend, light grey lines represent all data. Big circles represent days with temperature above 85th percentile. Average correlations of warmest summers with respect to each weather regime (black circle on x-axis).

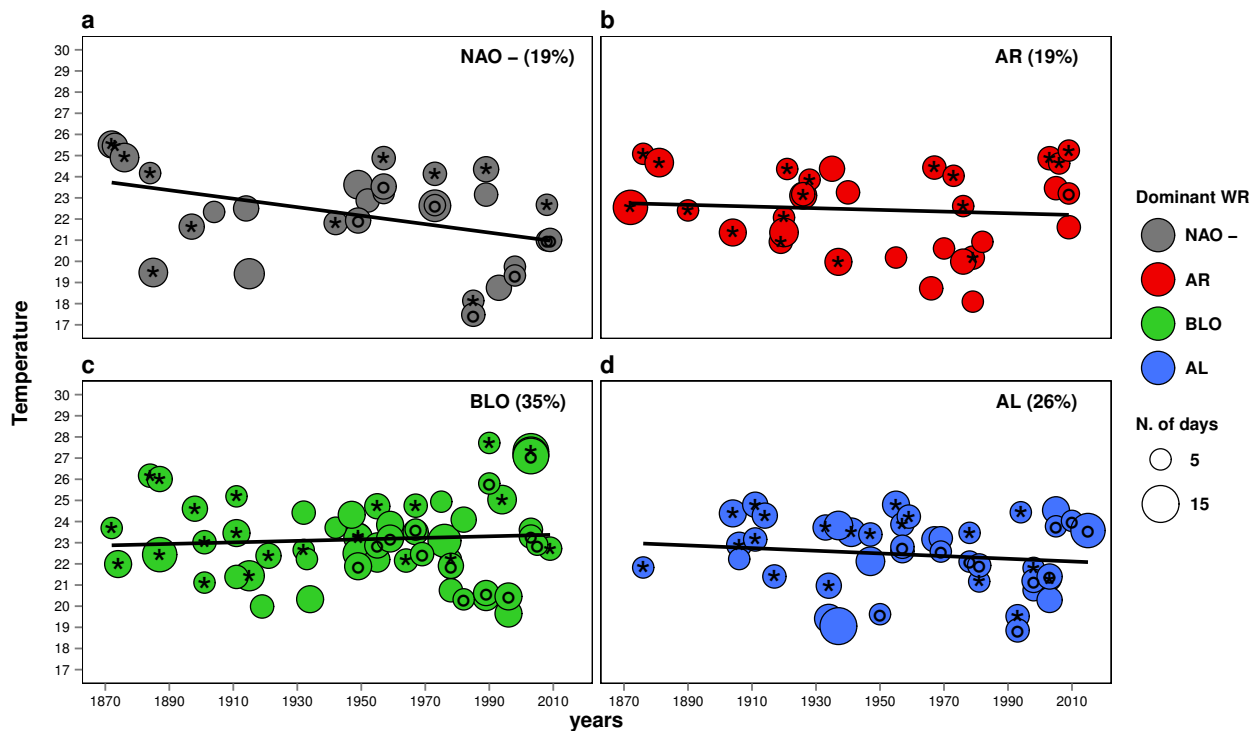


Figure 6. Dominant weather regimes during Summer Heatwave events in Western-Europe. Summer heatwave events (P90th Percentile) from 1871 to 2015 for different reanalysis products: 20CR (circle with stars), ERA20C (empty circle), and NCEP (circles with inner circle). Colors correspond to the dominant Weather regime (a-d,) in each event, temperature (y-axis) and years (x-axis). Circle sizes depend on the event duration by number of days, the larger the longer duration. Percentages show the frequency of each weather regime. Linear fits are shown in black solid lines.

Atmospheric dynamics leading to West European summer hot temperatures since 18719

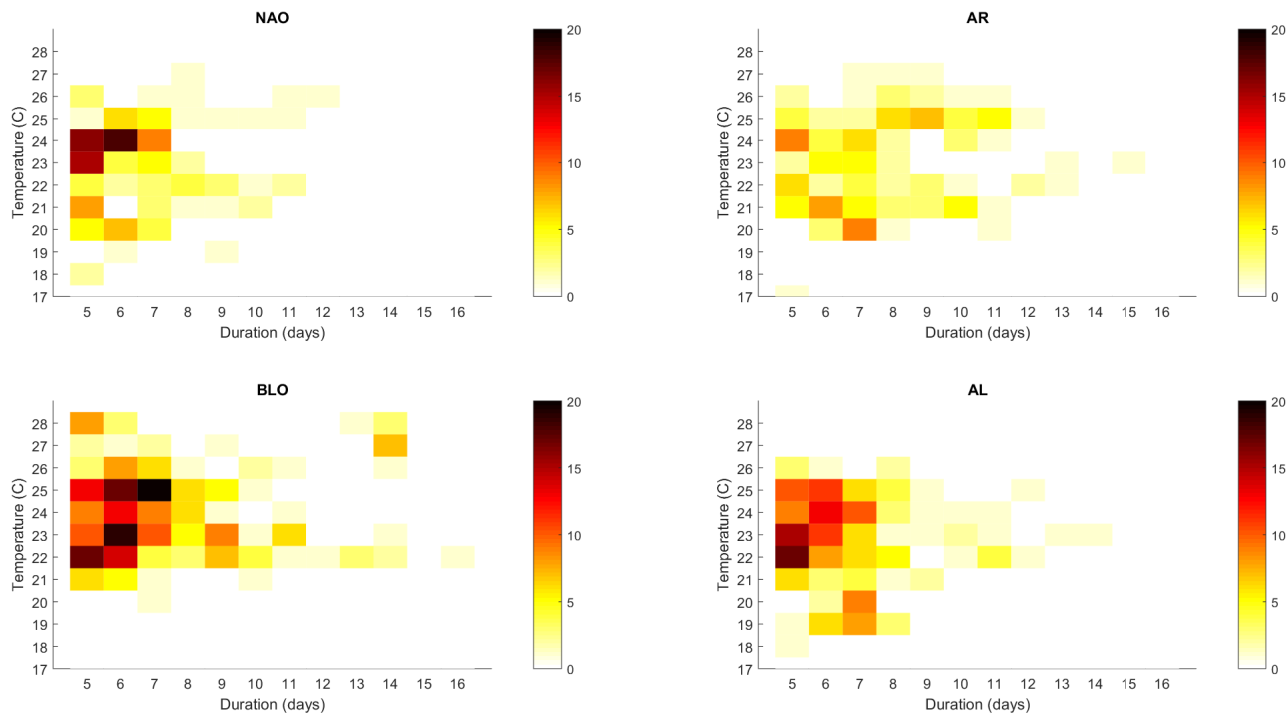


Figure 7. Density plot of heatwave events. Temperature (y-axis) vs numbers of days (x-axis) during each heatwave event for the 20CR Ensemble Mean (1871-2011) weather regimes. Colors represent the number of hetwaves events.

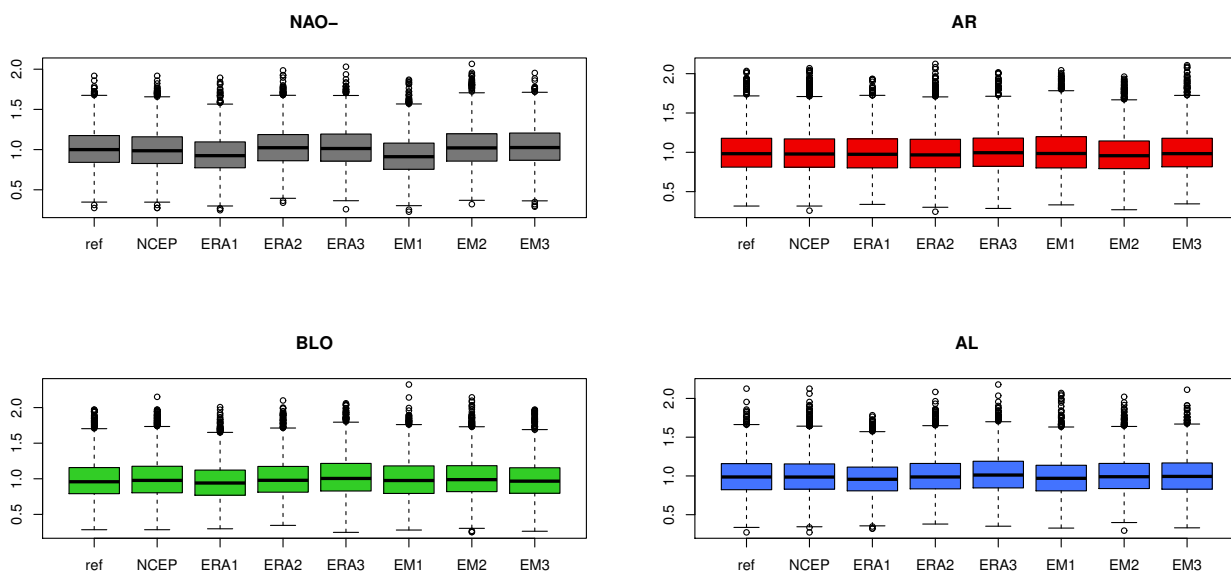


Figure 8. Boxplots of Absolute Root Mean Square Error by period and weather regime. Colors represent each weather regime. (See also Table S1).

Atmospheric dynamics leading to West European summer hot temperatures since 187110

Abs_{RMSE}	Period	NAO-	AR	BLO	AL
NCEP	(1970-2010)	1.01	1.00	0.98	0.99
	(1948-2015)	1.01	1.0	1.01	1.00
ERA 20C	(1900-1936)	0.95	0.99	0.96	0.97
	(1937-1973)	1.03	0.99	1.01	1.01
	(1974-2010)	1.03	1.01	1.03	1.03
20CR	(1871-1917)	0.94	1.01	1.00	0.99
	(1918-1964)	1.03	0.98	1.02	1.01
	(1965-2011)	1.04	1.01	0.99	1.01

Table 1. Absolute error of the Root mean square deviation (Abs_{RMSE}) of the truncated EOFs during the training period(NCEP:1970-2010) by Weather Regimes during summer in Western-Europe (see also Figure S8)

p-value	NAO-	AR	BLO	AL
M0	0.42	0.56	0.20	0.23
M1	0.57	0.53	0.23	0.32
M2	0.67	0.82	0.07	0.80
M3	0.88	0.74	0.09	0.87
M4	0.65	0.94	0.13	0.79
M5	0.81	0.91	0.09	0.54
M6	0.29	0.84	0.27	1.00
M7	0.18	0.53	0.30	0.80
M8	0.38	0.47	0.05	0.57
M9	0.71	0.63	0.45	0.81
EM 20CR	0.40	0.44	0.23	0.25
ERA 20C	0.32	0.37	0.30	0.65
NCEP	0.26	0.00	0.50	0.24
Mean 20C	0.54	0.67	0.19	0.63
Mean rea.	0.33	0.27	0.34	0.38

Table 2. p-values of Heatwave events calculate for each dataset and regime. Mean 20C is the mean of all the members with EM20CR (trend line in figure 3) and Mean rea. is the mean of all the reanalyses (EM20CR, ERA20C, NCEP) (trend line in figure S6). To calculate the p-values we fit a linear model. The null hypothesis is that there is no trend. The statistics and the degrees of freedom are evaluated as in Chamber, 1992 and Wilkinson an Rogers, 1973)

Periods	NAO-	AR	BLO	AL
Period 1 (30-days filter)	0.22	-0.1	-0.14	0.02
Period 2 (30-days filter)	-0.07	0.04	0.01	0.02
Period 3 (30-days filter)	-0.11	0.07	0.04	0.01
Period 1 (Without filter)	0.23	-0.11	-0.14	0.02
Period 2 (Without filter)	-0.08	0.01	0.05	0.03
Period 3 (Without filter)	-0.11	0.08	0.01	0.02

Table 3. Average correlations of hottest summers in figure 2. The three periods correspond to periods plotted in Fig.2 (NAO-, AR) and Fig. S4. (BLO, AL). The three first periods *30-days filter* show the average correlations of the warmest summers in 20CR plotted in the axis as black diamonds in Fig.2 and Fig. S4., applying a 30-days moving average filter for the warmest summers. The three periods *without filter* show the same information but without applying any filter.